THE JOURNAL OF PHYSICAL CHEMISTRY C

Article

pubs.acs.org/JPCC

Temperature and Voltage Dual-Responsive Ion Transport in Bilayer-Intercalated Layered Membranes with 2D Nanofluidic Channels

Tianliang Xiao,[†] Qingqing Liu,[†] Qianqian Zhang,[‡] Zhaoyue Liu,*[,†] and Jin Zhai*[,†]

[†]Key Laboratory of Bio-Inspired Smart Interfacial Science and Technology of Ministry of Education, School of Chemistry, and [‡]School of Physics and Nuclear Energy Engineering, Beihang University, Beijing 100191, P. R. China

Supporting Information

ABSTRACT: The controllable ion transport in synthetic membranes with nanofluidic channels by external stimuli has been attracting significant attention for nanofluidic diodes, biosensing, nanoreactors, and energy conversion. Here, we report a synthetic bilayer-intercalated layered membrane with two-dimensional (2D) nanofluidic channels, in which the ion transport can be controlled by external stimuli of temperature and voltage. The synthesis of the layered membranes includes the exchange of native cations in montmorillonite with the quaternary ammonium ions in a cationic surfactant and a subsequent vacuum filtration. The bilayer-intercalated interlayer spaces in the layered membranes act as 2D nanofluidic channels for ion transport. The phase state of the bilayers and the surface polarity of functionalized montmorillonite lamellae can be controlled by external temperature and voltage, respectively, which imbue the layered membranes with dual-responsive ion transport properties. Our dual-responsive layered membranes with 2D nanofluidic channels provide a new platform for creating smart synthetic membranes to control the ion transport.

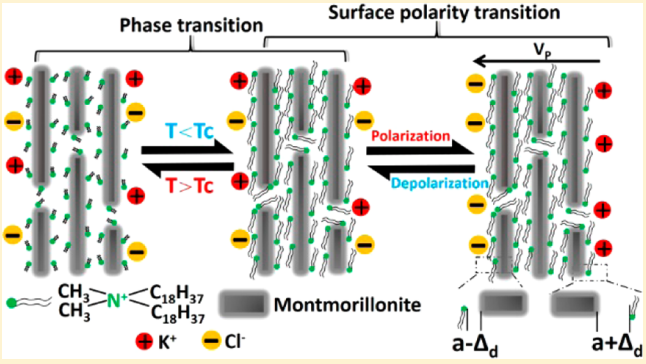

INTRODUCTION

Biological cell membranes embedded with ion channels play an indispensable role in life processes.[1] The biological function of cell membranes is often achieved by their controllable ion transport in ion channels responding to environmental stimuli such as voltage, pH, ions, light, and temperature.[2−6] Inspired by the function of biological membranes, the development of responsive synthetic membranes embedded with nanofluidic channels to control the ion transport has attracted considerable interest.[7−14] Compared with their biological counterparts, the responsive synthetic membranes feature several advantages of robust mechanical properties, excellent chemical stability, and great flexibility, which can be widely applied in an abiotic environment for nanofluidic diodes, biosensing, nanoreactors, and energy conversion.[15−22] Considerable efforts have been devoted to design and fabricate single-responsive synthetic membranes with single- or multi-nanofluidic channels.[23−32] However, considering the complex biological environment and the multiresponsiveness of biological membranes, synthetic membranes with dual- or multiresponsive character are indispensable. Compared with single-responsive systems, the dual-responsive synthetic membranes are more similar to biological membranes, which show potential application as sensors to detect dual external stimuli. Several kinds of synthetic membranes with ion transport responding to two kinds of stimuli have been built by modifying the embedded nanofluidic channels with two kinds of single-responsive molecules or a kind of dual-responsive molecule.[33−40] The stimuli-responsive change of surface charge or molecular conformation contributes to the dual-responsive characteristic. From the standpoint of mimicking the complex functions of biological membranes, the development of synthetic membranes with alternative dual-responsive characteristics is still of significant importance.

Layered membranes derived from the stacking of exfoliated two-dimensional (2D) lamellae have attracted significant interest for the fabrication of responsive synthetic membranes because the interlayer spaces between 2D lamellae can serve as native 2D nanofluidic channels to confine the transport of the ions and electrolytes.[41−47] The surface of 2D nanofluidic channels in layered membranes can be conveniently modified with functional molecules by controlling the component of 2D lamellae. For example, the surface charge polarity of 2D nanofluidic channels in layered graphene membranes can be reversed from negative to be positive by functionalization of 2D graphene lamellae with imidazolium cations.[48] However, to the best of our knowledge, synthetic membranes with a dual-responsive ion transport characteristic have not be achieved through the restacking of functionalized 2D lamellae.

Received: June 26, 2017
Revised: August 12, 2017
Published: August 14, 2017

DOI: 10.1021/acs.jpcc.7b06245
J. Phys. Chem. C 2017, 121, 18954−18961

Herein, we report a dual-responsive synthetic membrane with 2D nanofluidic channels derived from the stacking of amphiphile-functionalized 2D montmorillonite lamellae, in which the ion transport can be controlled by external stimuli of temperature and voltage. Montmorillonite is a cheap and easily available clay mineral with disordered layers composed of Al−O octahedral sheet sandwiched by two Si−O tetrahedral sheets.[49,50] The layers of montmorillonite can be exfoliated in water by exchanging their native cations with organic cations.[51,52] In this work, we use a cationic surfactant of dioctadecyldimethylammonium bromide to exfoliate montmorillonite into quaternary ammonium amphiphiles functionalized 2D lamellae. After the functionalized 2D montmorillonite lamellae are restacked into layered membranes by vacuum filtration, the interlayer spaces between montmorillonite lamellae are intercalated by quaternary ammonium bilayers, which act as 2D nanofluidic channels for ion transport. The phase state of the bilayers and the surface polarity of functionalized montmorillonite lamellae can be controlled by external temperature and voltage, respectively, which imbue the layered membranes with dual-responsive ion transport properties.

EXPERIMENTAL SECTION

Synthesis of Bilayer-Intercalated Layered Montmorillonite Membranes. The amphiphile-functionalized 2D montmorillonite lamellae were prepared by the exfoliation of layered montmorillonites using cationic surfactants in water.[53] Typically, a 40 mL aqueous suspension of 0.8 g of montmorillonite with an ion exchange capacity of 120 mequiv/100 g (Nanocor, USA) and a 10 mL aqueous dispersion of 0.68 g of dioctadecyldimethylammonium bromide (Aldrich) were mixed and then stirred at a temperature of 70 °C for 1 h. After being cooled to room temperature, the suspension was centrifuged at 2000 rpm, and light-yellow precipitates composed of amphiphile-functionalized 2D montmorillonite lamellae were obtained. The precipitates were then washed by a chloroform/methanol with volume ratio of 1:1 to remove the excessive surfactants. Finally, the precipitates were stirred in 50 mL of chloroform for 24 h to form a light-yellow suspension solution. A layered membrane was obtained by vacuum filtration of 10 mL of suspension solution through a nylon filter membrane (50 mm diameter and 0.45 μm pore size, Shanghai Xinya, China). After filtration, the layered membrane was then peeled off from the nylon filter, and a self-standing membrane was obtained.

Characterization. The morphology of exfoliated 2D montmorillonite lamellae was observed by a FEI JEM-1200EX transmission electron microscope (TEM). The thickness of exfoliated lamellae was measured using Bruker Dimension Icon atomic force microscope (AFM). A freshly cleaved mica sheet was used as a substrate for the AFM measurement. The surface and cross-sectional morphology of restacked layered membrane were observed using a FEI Quanta FEG 250 environmental scanning electron microscope (SEM). The contact angles (CAs) were measured using a POWEREACH JC2000D1 system (Shanghai Zhongchen, China) with Milli-Q water. The interlayer spacing of layered membranes was characterized by an Ultima IV X-ray diffraction meter (Rigaku Corporation, Japan). The d_{001} spacing of layered montmorillonite membrane was calculated according to Bragg's equation ($n\lambda = 2d \sin \theta$). The component of layered membranes and the phase transition temperature of the bilayers were measured by thermogravimetric analysis and differential scanning calorimetry (TGA/DSC, METTLER SF/1382, Switzerland) under a N_2 flow. The heating ramp for TGA and DSC measurements was 10 and 2 °C min^{-1}, respectively.

Electric Measurements. The ion transport in the 2D nanofluidic channels of layered membranes was studied by measuring the ion current−voltage ($I-V$) curves. As shown in Figure S1, the layered membrane was mounted between the two chambers of an electrochemical cell.[54] The effective area of the membrane for ion transport is about 0.2 cm^2. A KCl aqueous solution with a concentration of 1 mM was chosen as electrolyte. Two Ag/AgCl electrodes were used to apply a stable transmembrane voltage across the membrane. The ion current at scanned voltages was measured by a Keithley 6487 picoammeter (Keithley Instruments, Cleveland, OH). The temperature-responsive ion transport property of layered membranes was characterized by measuring the ion current in a 1 mM KCl electrolyte with a temperature ranging from 20 to 70 °C. We first added the electrolyte solution with a temperature of 70 °C into the electrochemical cell. Then, the electrolyte was cooled naturally, and its real temperature was measured by a thermometer. We measured the ion current−voltage ($I-V$) curves when the temperature of electrolyte was 20, 30, 40, 50, 60, and 70 °C. The ion conductivity of 1 mM KCl electrolyte at different temperatures was measured using a conductivity meter (Shanghai INESA Scientific Instrument, China). The ion conductance through the layered membrane in KCl electrolyte with different concentrations at room temperature was calculated from the $I-V$ curves at scanned voltages from −1 to +1 V. In order to characterize the voltage responsiveness, an external polarization voltage was applied across the layered membrane through two stable Pt electrodes for some time (Figure S2). The layered membrane was also mounted between the two chambers of an electrochemical cell filled with 1 mM KCl aqueous solution. After removing the external polarization voltage, the ion current was measured immediately through two Ag/AgCl electrodes at scanned voltages from −0.2 to +0.2 V (Figure S2). During all the experiments, the polarity of the voltage for polarizations and $I-V$ measurements remained the same.

RESULTS AND DISCUSSION

Because of the weak interlayer interaction and negative net layer charges, montmorillonite can be swelled and exfoliated into 2D lamellae in water by exchanging their native cations of Na^+, Ca^{2+}, and K^+ with the quaternary ammonium cations.[51,52] As shown in Figure 1, in our work, the exfoliation of montmorillonite is achieved by stirring a mixture of commercially available montmorillonite and a cationic surfactant of dioctadecyldimethylammonium bromide in water at 70 °C for 1 h.[53] After centrifugation, the resulted 2D montmorillonite lamellae can be stably dispersed in in a solvent of chloroform because of the functionalization of quaternary ammonium amphiphiles on the surface of montmorillonite. After vacuum filtration of the chloroform suspension solution using a nylon filter, a self-standing membrane is obtained as shown in Figure 1.

The dispersion of quaternary ammonium amphiphiles functionalized 2D montmorillonite lamellae in chloroform forms a stable colloidal suspension with a visible color of light yellow as shown in Figure 2A. The TEM image (Figure 2B) indicates that the exfoliated montmorillonite in chloroform shows a clear lamellar structure, which therefore can be used as

DOI: 10.1021/acs.jpcc.7b06245
J. Phys. Chem. C 2017, 121, 18954−18961

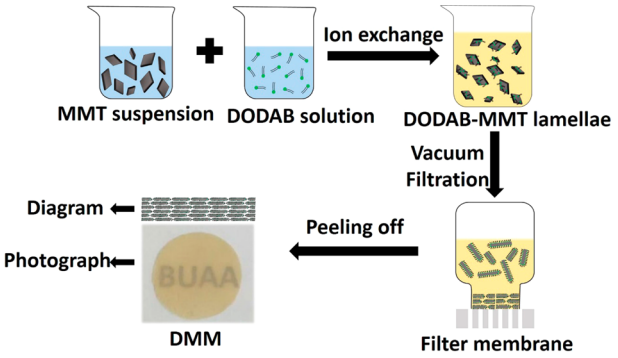

Figure 1. Flowchart for the fabrication of bilayer-intercalated layered montmorillonite membranes. The exchange of the native cations in montmorillonite (MMT) with the quaternary ammonium ions in dioctadecyldimethylammonium bromide (DODAB) resulted in amphiphile-functionalized 2D montmorillonite (DODAB–MMT) lamellae in chloroform. After vacuum filtration, the layered membrane was peeled off from the filter, and a self-standing DODAB–MMT membrane (DMM) was obtained.

an ideal building block for the formation of layered membranes. Figure 2C shows an AFM image of typical exfoliated montmorillonite lamellae on a freshly cleaved mica sheet, which also identifies a lamellar structure. The lateral dimensions of exfoliated 2D lamellae distribute in a large range from one to several hundred nanometers. The height profile in Figure 2C indicates that the thickness of the lamella is ~3.64 nm. From the X-ray diffraction (XRD) pattern of montmorillonite powders obtained by drying the exfoliated lamellae at room temperature and ambient pressure (Figure S3), it is calculated that the d_{001} spacing of montmorillonite is ~3.63 nm based on the diffraction peak at 2.4°, which is much larger than that in native montmorillonite (1.19 nm) because of the intercalation of quaternary ammonium ions.[55] The combination of AFM and XRD results indicates that the exfoliated 2D montmorillonite lamella has a single-layer structure. Based on the fact that the thickness of a single-layer native montmorillonite lamella is ~0.96 nm,[56] the total thickness of quaternary ammonium ions on the two sides of single-layer montmorillonite lamella is ~2.67 nm.

The exfoliated 2D montmorillonite lamella in chloroform can be restacked into light-yellow, paper-like membrane by vacuum filtration. The self-standing membrane is not swelled in water and shows a robust mechanical property and great flexibility as shown in Figure 3A and Figure S4. As a comparison, the membrane derived from native montmorillonite lamellae without functionalization of quaternary ammonium ions is

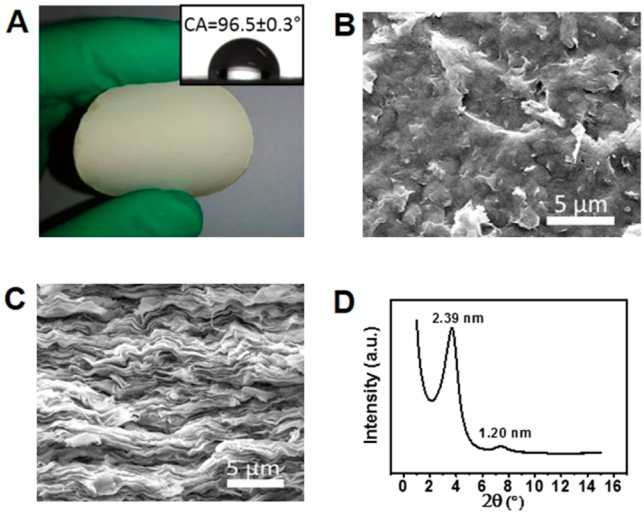

Figure 3. Characterizations of the bilayer-intercalated layered montmorillonite membranes. (A) Photograph of the self-standing and flexible layered membrane with a water contact angle of 96.5 ± 0.3°. (B, C) Top-view (B) and cross-sectional (C) SEM images. The self-standing membrane shows an oriental layered structure. (D) XRD pattern of restacked layered membranes (DMM). The d_{001} spacing of layered membrane is 2.39 nm.

swelled and broken while immersed in water (Figure S4), which indicates that the quaternary ammonium amphiphiles are indispensable for a stable montmorillonite membrane in water. The surface of layered membrane demonstrates hydrophobicity with a water contact angle of ~96.5° because of the exposed double octadecyl chains on the surface. The self-standing membrane demonstrates a smooth surface without obvious defects (Figure 3B). The wrinkles on the surface imply that the membrane comprises plenty of lamellae. The layered structure of the self-standing membrane is clearly observed from the cross-sectional SEM image as shown in Figure 3C. The 2D lamellae are stacked densely to form an oriental layered structure. The XRD pattern (Figure 3D) demonstrates that the calculated d_{001} spacing in layered membrane from the diffraction peak at 3.70° is 2.39 nm, which is much smaller than that (~3.63 nm) of the dried powders of exfoliated lamellae at room temperature and ambient pressure. It is considered that contractive d_{001} spacing should be related with the significant tilt of double octadecyl chains after vacuum filtration. After subtracting the thickness of a single-layer native montmorillonite lamella (~0.96 nm),[56] the interlayer spacing in layered membrane is estimated to be ~1.43 nm. The massive interlayer spaces in the layered membrane act as 2D nanofluidic

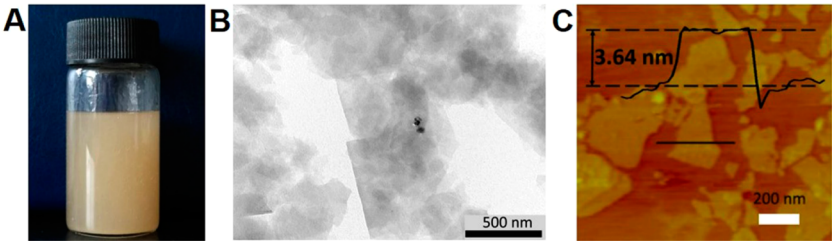

Figure 2. (A) Suspension of dioctadecyldimethylammonium bromide (DODAB)–montmorillonite (MMT) lamellae in chloroform is stable enough for restacking because of the hydrophobic double octadecyl chains on the surface of montmorillonite. (B) TEM image of the DODAB–MMT lamellae. (C) AFM image and corresponding height profile of DODAB–MMT lamellae shows that the lamella is a single-layer structure. The lateral dimensions of exfoliated lamellae vary from one to several hundred nanometers.

DOI: 10.1021/acs.jpcc.7b06245
J. Phys. Chem. C 2017, 121, 18954–18961

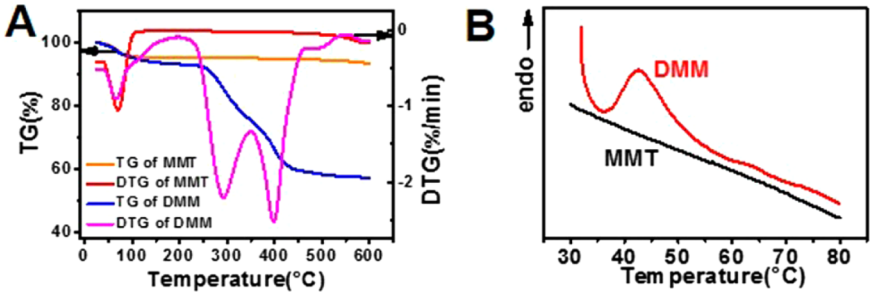

Figure 4. (A) TG and DTG plots of native montmorillonite (MMT) and restacked layered membranes (DMM), which proves the intercalation of quaternary ammonium ions. (B) DSC plot of MMT and DMM, showing that the phase transition temperature of quaternary ammonium bilayers is nearly 45 °C.

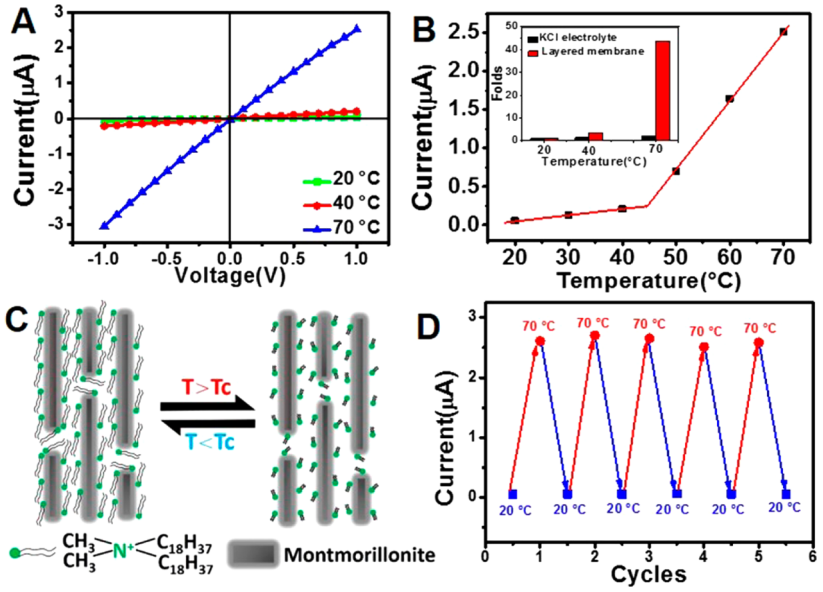

Figure 5. Temperature-responsive ion transport property of bilayer-intercalated layered montmorillonite membranes. (A) Representative *I*−*V* curves of the layered membranes in 1 mM KCl electrolyte with a temperature of 20, 40, and 70 °C. (B) Correlation of ion current at +1 V with the temperature. Inset: enhancement folds of the ion current at 40 and 70 °C when compared with that at 20 °C. As a comparison, the enhancement folds of theoretical ion current in 1 mM KCl electrolyte at +1 V is calculated from the ion conductivity of the electrolyte. The sharp increase of ion current at 45 °C is ascribed to the phase transition of quaternary ammonium bilayers. (C) Schematic diagram for the phase transition of the bilayer from a gel to liquid-crystalline state. The liquid-crystalline state is favorable for the transport of water-soluble ions. (D) Reversible and stable switch of ion current (at +1 V) at 20 and 70 °C for five cycles.

channels for ion transport. The content of organic quaternary ammonium ions in layered membranes is analyzed by thermogravimetric analysis (TGA) as shown in Figure 4A. Compared with native montmorillonite, the restacked layered membrane demonstrates a weight decrease of ∼36.2% in the temperature range from 240 to 600 °C, which is ascribed to the two-step thermal decomposition of quaternary ammonium ions as evidenced by the two peaks at 293 and 398 °C in the curves of differential thermogravimetric analysis (DTG). It has been well-known that the double-chain amphiphiles of quaternary ammonium ions can form bilayers in the interlayer space of restacked montmorillonite membrane.[57] On the basis of the bimolecular length of dioctadecyldimethyl quaternary ammonium ions (∼5.0 nm)[53] and the interlayer spacing of layered membrane (∼1.43 nm), we calculated the tilt angle of octadecyl chains in the interlayer space is ∼17°. The phase state of ammonium bilayers is dependent on the temperature. Based on the endothermic peak in the differential scanning calorimetry (DSC) patterns (Figure 4B), the phase transition temperature (T_c) of quaternary ammonium bilayers is determined to be ∼45 °C, which corresponds to the phase transition from an ordered gel to disordered liquid-crystalline state of bilayer.[58]

The ion transport in the 2D nanofluidic channels of layered membranes is identified by the measurements of ion conductance (Figure S5). At a high KCl concentration, the conductance through layered membranes decreases following the decrease of KCl concentration. However, when the KCl concentration is below 1 mM, the conductance remains constant, which is independent of KCl concentration. As a comparison, the conductance of bulk KCl electrolyte is proportional to its concentration. Our results indicate that the ion transport in the 2D nanofluidic channels of layered membranes is governed by the excessive surface negative charges of montmorillonite lamellae.[59] The temperature-dependent phase state of the quaternary ammonium bilayers in 2D nanofluidic channels of layered membrane can be used to control the ion transport. The ion transport property of layered membranes is characterized by measuring their ion current−voltage curves (*I*−*V*) in KCl electrolyte using a setup as shown in Figure S1. Figure 5A shows the typical *I*−*V* curves of a

DOI: 10.1021/acs.jpcc.7b06245
J. Phys. Chem. C 2017, 121, 18954−18961

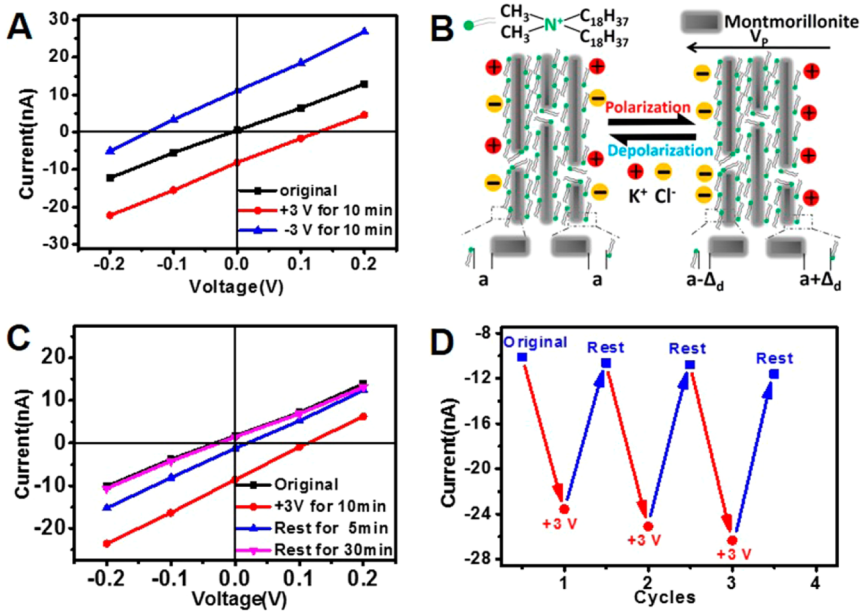

Figure 6. Voltage-responsive ion transport property of bilayer-intercalated layered montmorillonite membranes. (A) $I-V$ curves of the layered membrane before and after applied with an external voltage of +3 and −3 V for 10 min. An external voltage shifts the $I-V$ curve of the layered membrane. (B) Schematic diagram for the polarization effect of layered membranes under a positive external voltage. The position of quaternary ammonium cations (positive charges) deviates by a displacement of Δ_d from their original equilibrium position along the direction of electric field. The asymmetric accumulation of K^+ and Cl^- on the two sides of the membrane consequently creates an electrochemical potential difference. (C) $I-V$ curves of layered membrane after rest in electrolyte for 5 and 30 min when the external voltage of +3 V is removed. The $I-V$ curve recovers back to its original state after nearly 30 min rest because of the depolarization process. (D) Reversible and stable switch of ion current at −0.2 V when the layered membrane is polarized and depolarized for three cycles.

layered membrane (thickness = ∼63 μm, Figure S6) in KCl aqueous electrolyte (1 mM) with a temperature of 20, 40, and 70 °C. For a clear comparison, the correlation of ion current at +1 V with the temperature is plotted in Figure 5B. It is observed that the ion current in the layered membrane increases slowly following the increase of temperature from 20 to 45 °C. However, the ion current starts to increase sharply when the temperature is higher than 45 °C. At a typical temperature of 70 °C, the value of ion current at +1 V is 2.60 μA, which is almost 43 times as much as that (0.06 μA) at 20 °C (inset of Figure 5B). Note that the ion conductivity of 1 mM KCl electrolyte increases linearly with the temperature (Figure S7). When the temperature increases from 20 to 70 °C, the theoretical ion current in 1 mM KCl electrolyte at +1 V (without layered membrane) is enhanced by only 2 times when calculated from the ion conductivity of the electrolyte (inset of Figure 5B). Therefore, the temperature-responsive ion transport property in the layered membrane is not derived from the change of ion conductivity by temperature. We therefore concluded that the sharp increase of ion current at 45 °C should be related with the phase transition of quaternary ammonium bilayers in the 2D nanofluidic channels of layered membranes. As mentioned above, the phase transition temperature of bilayers is about ∼45 °C. When the temperature is lower than 45 °C, the bilayers in the layered membranes exist as a gel state, in which the double octadecyl chains are arranged densely and orderly (Figure 5C). The water-soluble ions are difficult to pass through the 2D nanofluidic channels, which results in a low ion current. The slow increase in the ion current by the temperature may be ascribed to the increase in the ion conductivity of electrolyte. When the temperature is higher than 45 °C, the state of quaternary ammonium bilayers transformed from a gel to liquid-crystalline phase. In this state, the arrangement of double octadecyl chains becomes disordered as shown in Figure 5C. The shrinking and bending of double octadecyl chains reduce the thickness of bilayers,[60] which is favorable for the transport of water-soluble ions and results in a high ion current. Furthermore, the reversible phase transition of bilayers between a gel and liquid-crystalline state results in a reversible temperature-responsiveness of ion current. As shown in Figure 5D and Figure S8, when the temperature of the electrolyte increases from 20 to 70 °C, the ion current at +1 V in the layered membrane increase from 0.06 to 2.60 μA. The decrease of temperature to be 20 °C recovers the ion current to be 0.06 μA. After five cycles, the ion current in the layered membrane at 20 and 70 °C remains almost unchanged, which indicates that the temperature-responsiveness of bilayer-intercalated layered membranes shows a good stability and reversibility.

Besides the temperature-responsive ion transport property, we also find that the ion transport in the layered membranes can be controlled by an external voltage. In order to characterize the voltage responsiveness, an external direct voltage was applied perpendicularly across the layered membrane through two stable Pt electrodes for 10 min (Figure S2). After removing the external voltage, the ion current was measured immediately through two Ag/AgCl electrodes at scanned voltages from −0.2 to +0.2 V (Figure S2). As shown in Figure 6A, after an external voltage of +3 V is applied across the membrane for 10 min, the $I-V$ curve of the layered membrane shows an almost parallel shift to the direction of negative current when compared with that of the original membrane. A positive voltage at zero current (V_{ZC}) and a negative current at zero voltage (I_{ZV}) are generated. The ion current at a negative voltage is enhanced by the external voltage, while an opposite result is observed at a positive voltage. An external voltage of

DOI: 10.1021/acs.jpcc.7b06245
J. Phys. Chem. C 2017, 121, 18954−18961

−3 V parallel shifts the $I-V$ curve to the direction of positive current. On the contrary, the ion current at a negative voltage is reduced by the external voltage, and the ion current at a positive voltage is enhanced. Our result indicates that the bilayer-intercalated layered membrane demonstrates a voltage-responsive ion transport property.

As shown in Figure 6B, in the bilayer-intercalated layered membrane, the negative charges of montmorillonite lamellae are balanced by the positive charges in quaternary ammonium ions after cationic exchange. The equilibrium distance between negative and positive charges is supposed to be a. Therefore, when the layered membrane is immersed into the KCl electrolyte, no potential difference is formed across the layered membrane because of its neutral surface. After an external voltage of +3 V is applied across the membrane, the charge balance is broken and a polarization effect occurs.[61] The positions of dioctadecyldimethylammonium cations (positive charges) on the surface of montmorillonite lamellae deviate by a displacement of Δ_d from their original equilibrium position along the direction of electric field (Figure 6B), while the positions of negative charges are considered to remain unchanged because they are fixed on the surface of montmorillonite lamellae. As a result, the side of montmorillonite membrane that faced to cathode shows electronegativity, while the surface that faced to anode shows electropositivity. After removing the external voltage, the electronegativity and electropositivity on the two sides of montmorillonite membrane are compensated by the cations (K^+) and anions (Cl^-) in the electrolyte, respectively. The asymmetric accumulation of K^+ and Cl^- on the two side of the membrane (Figure 6B) consequently creates an electrochemical potential difference (V_P in Figure 6B) with absolute value equal to the voltage at zero current (V_{ZC}) in the $I-V$ curve.[62]

The polarity of V_P is opposite with that of V_{ZC}, which therefore results in a negative ion current at zero voltage as shown in Figure 6A. When a transmembrane voltage (V_T) is applied across the layered membrane through two Ag/AgCl electrodes to measure the ion current, the actual voltage drop across the membrane is the algebraic sum of V_T and V_P ($V_T + V_P$). Considering the negative polarity of V_P, when the polarity of V_T is negative, the absolute value of actual voltage drop is higher than that of V_T, which enhances the generation of ion current. In the contrast, when the polarity of V_T is positive, the absolute value of actual voltage drop is lower than that of V_T, which results in a lower ion current than that of the original membrane. The degree of the polarization is dependent on the intensity of the external voltage and the polarization duration.[63] As shown in Figure S9, when the external voltage increases from +1 to +3 V while the polarization duration is fixed to be 10 min, the absolute value of polarization-induced potential difference (V_P) increases from 17.7 to 104.0 mV, which controls the ion current at −0.2 V from −13.5 to −22.8 nA. If the external voltage is fixed to be +3 V, the increase of polarization duration from 1 to 10 min shifts the absolute value of V_P from 32.2 to 104.0 mV, which controls the ion current at −0.2 V from −14.6 to −22.8 nA (Figure S10). Our results indicate that the ion transport in layered membranes can be controlled conveniently by the parameters of the external voltage.

Furthermore, the voltage responsiveness of layered membranes shows a stable reversibility. As shown in Figure 6C, after removing the external voltage of +3 V, the rest of the polarized membrane in the electrolyte eliminates slowly the voltage at zero current and the current at zero voltage because of the depolarization process. The $I-V$ curve almost recovers back to its original state after nearly 30 min. After the polarization and depolarization process is repeated three cycles, the ion current at −0.2 V remain almost unchanged (Figure 6D and Figure S11), which verifies that the voltage responsiveness of layered membrane shows an excellent stability and reversibility.

CONCLUSIONS

In summary, we have successfully fabricated a temperature and voltage dual-responsive synthetic layered membrane with 2D nanofluidic channels using bilayer-intercalated montmorillonite. The intercalation of quaternary ammonium bilayers is achieved by an exchange of dioctadecyldimethylammonium cations with the native cations of montmorillonite followed by a vacuum filtration. The reversible phase transition of quaternary ammonium bilayers in the 2D nanofluidic channels results in a temperature-responsive ion transport property. An external polarization voltage creates an electrochemical potential difference across the layered membrane, which is capable of controlling the ion transport in the 2D nanofluidic channels and results in a voltage-responsive ion transport property. Our dual-responsive synthetic layered membranes with 2D nanofluidic channels provide a new platform for creating smart synthetic membrane to control the ion transport.

ASSOCIATED CONTENT

Supporting Information

The Supporting Information is available free of charge on the ACS Publications website at DOI: 10.1021/acs.jpcc.7b06245.

Schematic setup for the measurement of ion current−voltage ($I-V$) curves and applying an external voltage across the layered membrane, XRD patterns of the powders of native montmorillonite (MMT) and functionalized montmorillonite (OMMT), the stability of two kinds of layered membranes, nanofluidic property of layered membrane, the low-magnified cross-sectional SEM image of a layered membrane, the ion conductivity of KCl aqueous solution (1 mM) of different temperature, $I-V$ curves of the layered membranes corresponding to temperature and voltage (PDF)

AUTHOR INFORMATION

Corresponding Authors

*E-mail: liuzy@buaa.edu.cn (Z.L.).
*E-mail: zhaijin@buaa.edu.cn. (J.Z.).

ORCID

Jin Zhai: 0000-0003-3596-411X

Notes

The authors declare no competing financial interest.

ACKNOWLEDGMENTS

This work was supported by National Key Research and Development Program of China (2017YFA0206902, 2017YFA0206900), National Natural Science Foundation of China (21571011, 21701003), National Basic Research Program of China (2014CB931803), and China Postdoctoral Science Foundation Grant (2015M580035, 2017T100022).

DOI: 10.1021/acs.jpcc.7b06245
J. Phys. Chem. C 2017, 121, 18954−18961

REFERENCES

(1) Hille, B. *Ion Channels of Excitable Membranes*; Sinauer: Sunderland, MA, 2001.

(2) Gadsby, D. C.; Kimura, J.; Noma, A. Voltage Dependence of Na/K Pump Current in Isolated Heart Cells. *Nature* **1985**, *315*, 63−65.

(3) Waldmann, R.; Champigny, G.; Bassilana, F.; Heurteaux, C.; Lazdunski, M. A Proton-Gated Cation Channel Involved in Acid-Sensing. *Nature* **1997**, *386*, 173−177.

(4) Voets, T.; Droogmans, G.; Wissenbach, U.; Janssens, A.; Flockerzi, V.; Nilius, B. The Principle of Temperature-Dependent Gating in Cold- and Heat-Sensitive TRP Channels. *Nature* **2004**, *430*, 748−754.

(5) Kato, H. E.; Inoue, K.; Abe-Yoshizumi, R.; Kato, Y.; Ono, H.; Konno, M.; Hososhima, S.; Ishizuka, T.; Hoque, M. R.; Kunitomo, H. Structural Basis for Na^+ Transport Mechanism by a Light-Driven Na^+ Pump. *Nature* **2015**, *521*, 48−53.

(6) Oortgiesen, M.; Van Kleef, R. G. D. M.; Vijverberg, H. P. M. Novel Type of Ion Channel Activated by Pb^{2+}, Cd^{2+}, and Al^{3+} in Cultured Mouse Neuroblastoma Cells. *J. Membr. Biol.* **1990**, *113*, 261−268.

(7) Siwy, Z.; Apel, P.; Baur, D.; Dobrev, D. D.; Korchev, Y. E.; Neumann, R.; Spohr, R.; Trautmann, C.; Voss, K. Preparation of Synthetic Nanopores with Transport Properties Analogous to Biological Channels. *Surf. Sci.* **2003**, *532*−*535*, 1061−1066.

(8) Martin, C. R.; Nishizawa, M.; Jirage, K.; Kang, M.; Lee, S. B. Controlling Ion-Transport Selectivity in Gold Nanotubule Membranes. *Adv. Mater.* **2001**, *13*, 1351−1362.

(9) Hou, X.; Guo, W.; Jiang, L. Biomimetic Smart Nanopores and Nanochannels. *Chem. Soc. Rev.* **2011**, *40*, 2385−2401.

(10) Siwy, Z. S.; Howorka, S. Engineered Voltage-Responsive Nanopores. *Chem. Soc. Rev.* **2010**, *39*, 1115−1132.

(11) Xu, Y.; Jiang, J.; Meng, Z.; Zhang, Q.; Li, X.; Zhai, J. Biomimic Redox Driven Ion Transportation in Smart Nanochannels. *J. Phys. Chem. C* **2016**, *120*, 17342−17347.

(12) Karnik, R.; Fan, R.; Yue, M.; Li, D.; Yang, P.; Majumdar, A. Electrostatic Control of Ions and Molecules in Nanofluidic Transistors. *Nano Lett.* **2005**, *5*, 943−948.

(13) Daiguji, H. Ion Transport in Nanofluidic Channels. *Chem. Soc. Rev.* **2010**, *39*, 901−911.

(14) Hou, X. Smart Gating Multi-Scale Pore/Channel-Based Membranes. *Adv. Mater.* **2016**, *28*, 7049−7064.

(15) Kalman, E. B.; Vlassiouk, I.; Siwy, Z. S. Nanofluidic Bipolar Transistors. *Adv. Mater.* **2008**, *20*, 293−297.

(16) Wen, L.; Hou, X.; Tian, Y.; Nie, F.; Song, Y.; Zhai, J.; Jiang, L. Bioinspired Smart Gating of Nanochannels Toward Photoelectric-Conversion Systems. *Adv. Mater.* **2010**, *22*, 1021−1024.

(17) Ali, M.; Tahir, M. N.; Siwy, Z.; Neumann, R.; Tremel, W.; Ensinger, W. Hydrogen Peroxide Sensing with Horseradish Peroxidase-Modified Polymer Single Conical Nanochannels. *Anal. Chem.* **2011**, *83*, 1673−1680.

(18) Gao, J.; Guo, W.; Feng, D.; Wang, H.; Zhao, D.; Jiang, L. High-Performance Ionic Diode Membrane for Salinity Gradient Power Generation. *J. Am. Chem. Soc.* **2014**, *136*, 12265−12272.

(19) Zhang, Q.; Xiao, T.; Yan, N.; Liu, Z.; Zhai, J.; Diao, X. Alternating Current Output from a Photosynthesis-Inspired Photoelectrochemical Cell. *Nano Energy* **2016**, *28*, 188−194.

(20) Xue, S.; Yeh, L. H.; Ma, Y.; Qian, S. Tunable Streaming Current in a pH-Regulated Nanochannel by a Field Effect Transistor. *J. Phys. Chem. C* **2014**, *118*, 6090−6099.

(21) Cheng, L.; Guo, L. J. Ionic Current Rectification, Breakdown, and Switching in Heterogeneous Oxide Nanofluidic Devices. *ACS Nano* **2009**, *3*, 575−584.

(22) Lin, L.; Yan, J.; Li, J. Small-Molecule Triggered Cascade Enzymatic Catalysis in Hour-Glass Shaped Nanochannel Reactor for Glucose Monitoring. *Anal. Chem.* **2014**, *86*, 10546−10551.

(23) Siwy, Z.; Heins, E.; Harrell, C. C.; Kohli, P.; Martin, C. R. Conical-Nanotube Ion-Current Rectifiers: The Role of Surface Charge. *J. Am. Chem. Soc.* **2004**, *126*, 10850−10851.

(24) Harrell, C. C.; Kohli, P.; Siwy, Z.; Martin, C. R. DNA−Nanotube Artificial Ion Channels. *J. Am. Chem. Soc.* **2004**, *126*, 15646−15647.

(25) Powell, M. R.; Sullivan, M.; Vlassiouk, I.; Constantin, D.; Sudre, O.; Martens, C. C.; Eisenberg, R. S.; Siwy, Z. S. Nanoprecipitation-Assisted Ion Current Oscillations. *Nat. Nanotechnol.* **2008**, *3*, 51−57.

(26) Wang, G.; Bohaty, A. K.; Zharov, I.; White, H. S. Photon Gated Transport at the Glass Nanopore Electrode. *J. Am. Chem. Soc.* **2006**, *128*, 13553−13558.

(27) Yameen, B.; Ali, M.; Neumann, R.; Ensinger, W.; Knoll, W.; Azzaroni, O. Synthetic Proton-Gated Ion Channels via Single Solid-State Nanochannels Modified with Responsive Polymer Brushes. *Nano Lett.* **2009**, *9*, 2788−2793.

(28) Li, C.; Ma, F.; Wu, Z.; Gao, H.; Shao, W.; Wang, K.; Xia, X. Solution-pH-Modulated Rectification of Ionic Current in Highly Ordered Nanochannel Arrays Patterned with Chemical Functional Groups at Designed Positions. *Adv. Funct. Mater.* **2013**, *23*, 3836−3844.

(29) Ali, M.; Ramirez, P.; Nguyen, H. Q.; Nasir, S.; Cervera, J.; Mafe, S.; Ensinger, W. Single Cigar-Shaped Nanopores Functionalized with Amphoteric Amino Acid Chains: Experimental and Theoretical Characterization. *ACS Nano* **2012**, *6*, 3631−3640.

(30) Zhang, Q.; Hu, Z.; Liu, Z.; Zhai, J.; Jiang, L. Light-Gating Titania/Alumina Heterogeneous Nanochannels with Regulatable Ion Rectification Characteristic. *Adv. Funct. Mater.* **2014**, *24*, 424−431.

(31) Xu, Y.; Sui, X.; Guan, S.; Zhai, J.; Gao, L. Olfactory Sensory Neuron-Mimetic CO_2 Activated Nanofluidic Diode with Fast Response Rate. *Adv. Mater.* **2015**, *27*, 1851−1855.

(32) Li, P.; Xie, G.; Kong, X.; Zhang, Z.; Xiao, K.; Wen, L.; Jiang, L. Light-Controlled Ion Transport through Biomimetic DNA-Based Channels. *Angew. Chem., Int. Ed.* **2016**, *55*, 15637−15641.

(33) Zhang, M.; Hou, X.; Wang, J.; Tian, Y.; Fan, X.; Zhai, J.; Jiang, L. Light and pH Cooperative Nanofluidic Diode Using a Spiropyran-Functionalized Single Nanochannel. *Adv. Mater.* **2012**, *24*, 2424−2428.

(34) Liu, M.; Zhang, H.; Li, K.; Heng, L.; Wang, S.; Tian, Y.; Jiang, L. A Bio-inspired Potassium and pH Responsive Double-gated Nanochannel. *Adv. Funct. Mater.* **2015**, *25*, 421−426.

(35) Liu, Q.; Xiao, K.; Wen, L.; Lu, H.; Liu, Y.; Kong, X.; Xie, G.; Zhang, Z.; Bo, Z.; Jiang, L. Engineered Ionic Gates for Ion Conduction Based on Sodium and Potassium Activated Nanochannels. *J. Am. Chem. Soc.* **2015**, *137*, 11976−11983.

(36) Perez-Mitta, G.; Marmisolle, W. A.; Trautmann, C.; Toimil-Molares, M. E.; Azzaroni, O. Nanofluidic Diodes with Dynamic Rectification Properties Stemming from Reversible Electrochemical Conversions in Conducting Polymers. *J. Am. Chem. Soc.* **2015**, *137*, 15382−15385.

(37) Zhang, Z.; Xie, G.; Xiao, K.; Kong, X.; Li, P.; Tian, Y.; Wen, L.; Jiang, L. Asymmetric Multifunctional Heterogeneous Membranes for pH- and Temperature-Cooperative Smart Ion Transport Modulation. *Adv. Mater.* **2016**, *28*, 9613−9619.

(38) Newton, M. R.; Bohaty, A. K.; Zhang, Y.; White, H. S.; Zharov, I. pH- and Ionic Strength-Controlled Cation Permselectivity in Amine-Modified Nanoporous Opal Films. *Langmuir* **2006**, *22*, 4429−4432.

(39) Buchsbaum, S. F.; Nguyen, G.; Howorka, S.; Siwy, Z. S. DNA-Modified Polymer Pores Allow pH- and Voltage-Gated Control of Channel Flux. *J. Am. Chem. Soc.* **2014**, *136*, 9902−9905.

(40) Zhang, Q.; Liu, Z.; Wang, K.; Zhai, J. Organic/Inorganic Hybrid Nanochannels Based on Polypyrrole-Embedded Alumina Nanopore Arrays: pH- and Light-Modulated Ion Transport. *Adv. Funct. Mater.* **2015**, *25*, 2091−2098.

(41) Shao, J.; Raidongia, K.; Koltonow, A. R.; Huang, J. Self-Assembled Two-Dimensional Nanofluidic Proton Channels with High Thermal Stability. *Nat. Commun.* **2015**, *6*, 7602.

(42) Stein, D.; Kruithof, M.; Dekker, C. Surface-Charge-Governed Ion Transport in Nanofluidic Channels. *Phys. Rev. Lett.* **2004**, *93*, 035901.

(43) Raidongia, K.; Huang, J. Nanofluidic Ion Transport through Reconstructed Layered Materials. *J. Am. Chem. Soc.* **2012**, *134*, 16528−16531.

DOI: 10.1021/acs.jpcc.7b06245
J. Phys. Chem. C 2017, 121, 18954−18961

(44) Guo, W.; Cheng, C.; Wu, Y.; Jiang, Y.; Gao, J.; Li, D.; Jiang, L. Bio-Inspired Two-Dimensional Nanofluidic Generators Based on a Layered Graphene Hydrogel Membrane. *Adv. Mater.* **2013**, *25*, 6064−6068.
(45) Miansari, M.; Friend, J. R.; Banerjee, P.; Majumder, M.; Yeo, L. Y. Graphene-Based Planar Nanofluidic Rectifiers. *J. Phys. Chem. C* **2014**, *118*, 21856−21865.
(46) Cheng, C.; Jiang, G.; Garvey, C. J.; Wang, Y.; Simon, G. P.; Liu, J.; Li, D. Ion Transport in Complex Layered Graphene-Based Membranes with Tuneable Interlayer Spacing. *Sci. Adv.* **2016**, *2*, e1501272.
(47) Wang, L.; Feng, Y.; Zhou, Y.; Jia, M.; Wang, G.; Guo, W.; Jiang, L. Photo-Switchable Two-Dimensional Nanofluidic Ionic Diodes. *Chem. Sci.* **2017**, *8*, 4381−4386.
(48) Ji, J.; Kang, Q.; Zhou, Y.; Feng, Y.; Chen, X.; Yuan, J.; Guo, W.; Wei, Y.; Jiang, L. Osmotic Power Generation with Positively and Negatively Charged 2D Nanofluidic Membrane Pairs. *Adv. Funct. Mater.* **2017**, *27*, 1603623.
(49) Narayanan, B. N.; Koodathil, R.; Gangadharan, T.; Yaakob, Z.; Saidu, F. K.; Chandralayam, S. Preparation and Characterization of Exfoliated Polyaniline/Montmorillonite Nanocomposites. *Mater. Sci. Eng., B* **2010**, *168*, 242−244.
(50) Shi, J.; Liu, H.; Lou, Z.; Zhang, Y.; Meng, Y.; Zeng, Q.; Yang, M. Effect of Interlayer Counterions on the Structures of Dry Montmorillonites with Si^{4+}/Al^{3+} Substitution. *Comput. Mater. Sci.* **2013**, *69*, 95−99.
(51) Xi, Y.; Frost, R. L.; He, H. Modification of the Surfaces of Wyoming Montmorillonite by the Cationic Surfactants Alkyl Trimethyl, Dialkyl Dimethyl, and Trialkyl Methyl Ammonium Bromides. *J. Colloid Interface Sci.* **2007**, *305*, 150−158.
(52) Xie, W.; Gao, Z.; Pan, W.; Hunter, D.; Singh, A.; Vaia, R. Thermal Degradation Chemistry of Alkyl Quaternary Ammonium Montmorillonite. *Chem. Mater.* **2001**, *13*, 2979−2990.
(53) Okahata, Y.; Shimizu, A. Preparation of Bilayer-Intercalated Clay Films and Permeation Control Responding to Temperature, Electric Field, and Ambient pH Changes. *Langmuir* **1989**, *5*, 954−959.
(54) Zhang, Q.; Liu, Z.; Hou, X.; Fan, X.; Zhai, J.; Jiang, L. Light-Regulated Ion Transport through Artificial Ion Channels Based on TiO_2 Nanotubular Arrays. *Chem. Commun.* **2012**, *48*, 5901−5903.
(55) He, H.; Ma, Y.; Zhu, J.; Yuan, P.; Qing, Y. Organoclays Prepared from Montmorillonites with Different Cation Exchange Capacity and Surfactant Configuration. *Appl. Clay Sci.* **2010**, *48*, 67−72.
(56) Sun, H.; Zhang, J.; Li, L.; Xu, J.; Sun, D. Surface Modification of Natural Na-Nontmorillonite in Alkane Solvents Using a Quaternary Ammonium Surfactant. *Colloids Surf., A* **2013**, *426*, 26−32.
(57) Kunjappu, J. T.; Somasundaran, P. Recent Trends in Bilayer Formation of Synthetic Amphiphiles. *Colloids Surf., A* **1996**, *117*, 1−5.
(58) Feitosa, E.; Barreleiro, P. C. A.; Olofsson, G. Phase Transition in Dioctadecyldimethylammonium Bromide and Chloride Vesicles Prepared by Different Methods. *Chem. Phys. Lipids* **2000**, *105*, 201−213.
(59) Bhattacharyya, K. G.; Gupta, S. S. Adsorption of a Few Heavy Metals on Natural and Modified Kaolinite and Montmorillonite: A Review. *Adv. Colloid Interface Sci.* **2008**, *140*, 114−131.
(60) Wu, F.; Wang, N.; Yu, Z. Nonsynchronous Change in the Head and Tail of Dioctadecyldimethylammonium Bromide Molecules during the Liquid Crystalline to Coagel Phase Transformation Process. *Langmuir* **2009**, *25*, 13394−13401.
(61) Kobayashi, K.; Horiuchi, S.; Kumai, R.; Kagawa, F.; Murakami, Y.; Tokura, Y. Electronic Ferroelectricity in a Molecular Crystal with Large Polarization Directing Antiparallel to Ionic Displacement. *Phys. Rev. Lett.* **2012**, *108*, 237601.
(62) Miansari, M.; Friend, J. R.; Yeo, L. Y. Enhanced Ion Current Rectification in 2D Graphene-Based Nanofluidic Devices. *Adv. Sci.* **2015**, *2*, 1500062.
(63) Armstrong, C. M.; Hille, B. The Inner Quaternary Ammonium Ion Receptor in Potassium Channels of the Node of Ranvier. *J. Gen. Physiol.* **1972**, *59*, 388−400.

DOI: 10.1021/acs.jpcc.7b06245
J. Phys. Chem. C 2017, 121, 18954−18961